Structural basis for Sec-independent membrane protein insertion by YidC

Kaoru Kumazaki[1,2*], Shinobu Chiba[3*], Mizuki Takemoto[1,2], Arata Furukawa[4], Ken-ichi Nishiyama[5], Yasunori Sugano[4], Takaharu Mori[6], Naoshi Dohmae[2], Kunio Hirata[7], Yoshiko Nakada-Nakura[8], Andrés D. Maturana[9], Yoshiki Tanaka[4], Hiroyuki Mori[10], Yuji Sugita[6], Fumio Arisaka[11], Koreaki Ito[3], Ryuichiro Ishitani[1,2], Tomoya Tsukazaki[4,12†] and Osamu Nureki[1,2†]

[1]Department of Biophysics and Biochemistry, Graduate School of Science, The University of Tokyo, 7-3-1 Hongo, Bunkyo-ku, Tokyo 113-0033, Japan; [2]Global Research Cluster, RIKEN, 2-1 Hirosawa, Wako-shi, Saitama 351-0198, Japan; [3]Faculty of Life Sciences, Kyoto Sangyo University, Motoyama, Kamigamo, Kita-ku, Kyoto 603-8555, Japan; [4]Department of Systems Biology, Graduate School of Biological Sciences, Nara Institute of Science and Technology, 8916-5, Takayama-cho, Ikoma, Nara 630-0192, Japan; [5]Cryobiofrontier Research Center, Faculty of Agriculture, Iwate University, 3-18-8 Ueda, Morioka, Iwate 020-8550, Japan; [6]Theoretical Molecular Science Laboratory, RIKEN, 2-1 Hirosawa, Wako-shi, Saitama 351-0198, Japan; [7]SR Life Science Instrumentation Unit, RIKEN SPring-8 Center, 1-1-1 Kouto, Sayo-cho, Sayo-gun, Hyogo 679-5148, Japan; [8]Department of Cell Biology, Graduate School of Medicine, Kyoto University, Yoshidakonoe-cho, Sakyo-ku, Kyoto 606-8501, Japan; [9]Department of Bioengineering Sciences, Graduate School of Bioagricultural Sciences, Nagoya University, Furo-cho, Chikusa-ku, Nagoya 464-8601, Japan; [10]Institute for Virus Research, Kyoto University, Shogoin Kawara-cho, Sakyo-ku, Kyoto 606-8507, Japan; [11]Graduate School of Bioscience and Biotechnology, Tokyo Institute of Technology, Nagatsuta-cho, Midori-ku, Yokohama, Kanagawa 226-8503, Japan; [12]JST, PRESTO, 4-1-8 Honcho, Kawaguchi, Saitama 332-0012, Japan

*These authors contributed equally to this work.

†To whom correspondence should be addressed.

Osamu Nureki: Phone: +81-3-5841-4392; E-mail: nureki@biochem.s.u-tokyo.ac.jp or Tomoya Tsukazaki: Phone: +81-743-72-5551; E-mail: ttsukaza@bs.naist.jp

Accurate insertion, folding and assembly of newly synthesized membrane proteins are critical for their functions. The YidC/Oxa1/Alb3 family proteins insert their substrates into the membrane, thereby facilitating membrane protein assembly in bacteria, mitochondria and chloroplasts[1,2]. In the bacterial cytoplasmic membrane, YidC functions as an independent insertase and a membrane chaperone in cooperation with the SecYEG-translocon[3–5]. Here we present the crystal structure of YidC from *Bacillus halodurans*, at 2.4 Å resolution. The structure revealed a novel fold, where five conserved transmembrane helices form a positively-charged hydrophilic groove open toward both the lipid bilayer and cytoplasm, but closed on the extracellular side. Structure-based *in vivo* analyses revealed that the conserved Arg residue in the groove is important for membrane protein insertion by YidC. We propose an insertion mechanism for single-spanning membrane proteins, in which the hydrophilic environment generated by the groove recruits the extracellular regions of substrates into the low-dielectric environment of the membrane.

The Sec translocon, a protein-conducting channel conserved in all three phylogenetic domains, translocates secretory proteins across the membrane and inserts membrane proteins *via* an hourglass-shaped pore formed by ten TM helices[6–8]. In

bacteria, YidC is another membrane protein involved in the insertion and folding of many membrane proteins[9–15], such as subunit c of the F_1F_o-ATPase (F_oc), and thus is essential for cell viability[3–5]. YidC is considered to function as both a Sec-dependent membrane chaperone and a Sec-independent insertase. In the latter Sec-independent pathway, YidC directly interacts with the translating ribosome to mediate the insertion of several single or double membrane-spanning proteins[16,17]. Previous studies suggested that YidC forms a face-to-face dimer to create a channel within its dimer interface[16,18], whereas another group reported that a monomer of membrane-embedded YidC is sufficient for binding to the substrate-translating ribosome[19]. In addition, Oxa1, the mitochondrial homologue of YidC, reportedly functions as a voltage-gated membrane channel, as well as a membrane protein insertase, probably by forming a tetramer[20]. However, the lack of a high-resolution structure of YidC has limited our understanding of the molecular mechanism of YidC-mediated membrane protein insertion.

Members of the genus *Bacillus* have two *yidC* genes, encoding YidC1 and YidC2. We determined the crystal structures of two constructs of *Bacillus halodurans* YidC2 (BhYidC $_{27–266}$ and BhYidC$_{27–267}$), which lack both the N-terminal signal and C-terminal non-conserved sequences (Fig. 1, Extended Data Table 1 and Extended Data Figs. 1, 2). A similar deletion variant of *B. subtilis* SpoIIIJ (YidC1), an ortholog of

BhYidC sharing 49.6% sequence identity, has comparable activity to the full-length protein *in vivo* (K248stop in Fig. 2a). Although the crystallographic asymmetric units of $BhYidC_{27–266}$ and $BhYidC_{27–267}$ contain one and two BhYidC molecules, respectively, the molecules in the crystalline lattice do not appear to form an effective oligomer, such as a face-to-face dimer[16,18] (Extended Data Fig. 3a, b). Recent fluorescence correlation spectroscopy and cryo-electron microscopy analyses of YidC bound to a translating ribosome showed that YidC exists as a monomer in detergent solution and in lipid membranes[17,19]. Consistently, our analysis using size exclusion chromatography coupled to multiangle laser light scattering (SEC-MALLS) also showed that BhYidC exists as a monomer in detergent solution (Extended Data Fig. 3c–e). Since the overall structures of $BhYidC_{27–266}$ and $BhYidC_{27–267}$ are nearly identical (r.m.s.d. 1.79 Å over residues 27–266), we mainly describe the structure of $BhYidC_{27–266}$.

The BhYidC structure consists of the N-terminal E1 region, the C-terminal C3 tail, and the core region, composed of TM helices 1–5, connected by two cytoplasmic (C1 and C2) and two extracellular (E2 and E3) regions (Fig. 1c). The E1 region consists of the EH1 helix, while the C1 region forms a hairpin-like structure composed of two helices (CH1 and CH2) connected by a short loop. The residues in the C2 region and the C3 tail are structurally disordered. The EH1, CH1 and CH2 helices protrude from the

core region, and lie nearly parallel to the plane of the membrane. The EH1 helix is amphipathic, while the CH1 and CH2 helices contain mainly hydrophilic residues. This observation suggested that one face of the EH1 helix is embedded in the membrane, while the CH1 and CH2 helices are exposed to the solvent (Fig. 1a). This notion is also consistent with theoretical calculations using the implicit membrane model (see Methods).

A comparison of the present structures of $BhYidC_{27–266}$ and $BhYidC_{27–267}$ suggested the flexibility of the C1 region, which does not interact with the other part of YidC (Extended Data Fig. 4a–c). The CH1 helix forms a continuous helix with the TM1 helix, which is kinked at the conserved Pro residues, Pro78 and Pro94 (Fig. 1c). The Pro residues and the partially disordered flexible loop connecting the CH2 and TM2 helices (residues 130–140), which may be embedded in the membrane, could enhance the flexibility of the C1 region. Indeed, this C1 region has higher B-factors than the other regions (Extended Data Fig. 5a). The results of the molecular dynamics (MD) simulation also suggested that the C1 region highly fluctuates in the lipid bilayer environment (Extended Data Fig. 6a, b).

To further investigate the functional importance of the C1 region, we performed the structure-based genetic analysis of *B. subtilis* SpoIIIJ. The membrane

insertion of MifM, a single-spanning membrane protein, is mediated by the YidC/SpoIIIJ pathway[21]. In this analysis, we measured the β-galactosidase (LacZ) activity of the YidC2-LacZ translational fusion, which is increased in response to a defect in the SpoIIIJ-dependent insertion of MifM (Extended Data Figs. 7a and 8). The two C1-deletion mutants (Extended Data Fig. 7b) exhibited elevated LacZ activities (Fig. 2a), suggesting that the C1 region is critical for the YidC-mediated membrane insertion of MifM. We then performed a growth complementation analysis using *B. subtilis* (the detail is described in the legend for Extended Data Fig. 7c). The results also suggested that the C1 region is important for the SpoIIIJ activity (Fig. 2b).

The extracellular halves of the TM1–5 helices, including the E2 region, are tightly packed with their hydrophobic side chains (Extended Data Fig. 5b, c), while the cytosolic halves of the TM1–5 helices loosely interact with each other to form a groove (~2,000 $Å^3$). This groove contains many hydrophilic residues, including the conserved Thr68, Arg72, Gln82, Gln142, Gln187, Asn248 and Gln254 residues, and thus generates a hydrophilic environment in the lipid bilayer (Fig. 2c and Extended Data Fig. 1). The conserved Arg72 residue, the only charged residue in this groove, protrudes into the center of this groove, and creates a strong positive electrostatic potential in the groove (Fig. 1b, d). This hydrophilic groove is open to both the cytosolic side and membrane

interior. In contrast, this groove is sealed toward the extracellular side by the hydrophobic core, and is not accessible from that side (Fig. 1d). The hydrophobic core, consisting of the hydrophobic residues in the extracellular half of BhYidC, has lower B-factors than the other regions, suggesting its rigidity (Extended Data Fig. 5). The structure-based genetic analyses suggested the importance of this hydrophobic core for the function of YidC (Fig. 2a–c and Extended Data Fig. 7b). A comparison of the $BhYidC_{27–266}$ and $BhYidC_{27–267}$ structures revealed that the groove in $BhYidC_{27–267}$ is narrower than that in $BhYidC_{27–266}$, suggesting the structural flexibility of the groove (Extended Data Fig. 4d). The results of the MD simulation also suggested that the size of the hydrophilic groove slightly fluctuates during the 1-μs simulation (Extended Data Fig. 6a). In contrast, the overall architecture of the core region, and the structure of the hydrophilic groove, remained rather stable in the lipid bilayer (Extended Data Fig. 6b), and the groove was constantly filled with ~20 water molecules (Extended Data Fig. 6c). The extracellular side of the groove remained sealed by the hydrophobic protein residues and the aliphatic lipid chains, and thus was impermeable to ions and water molecules during the simulation. Taken together, YidC could provide a flexible, hydrophilic groove in the membrane, which is open toward both the cytoplasmic side and membrane interior, and tightly sealed on the extracellular side.

To investigate the functional importance of the hydrophilic groove, we examined the membrane insertion activities of mutants of Arg73 (Arg72 in BhYidC, in Fig. 2c) and conserved Gln residues of SpoIIIJ by *in vivo* genetic analyses (Fig. 2c). The mutations of Arg73 abolished the MifM-insertion activity, except for R73K, which slightly decreased the activity (Fig. 2d). None of the mutants of Arg73, except for R73K, complemented the growth of the *spoIIIJ* mutant cells (Fig. 2b). In contrast, none of the Ala mutations of Gln83, Gln140, Gln187, and Gln238 (Gln82, Gln142, Gln187, and Gln254, respectively, in BhYidC, in Fig. 2c) had any effects on the MifM-insertion activity (Fig. 2e). A similar result was obtained for a chimaera between Pf3 coat protein, another single-spanning membrane protein inserted *via* the Sec-independent pathway, and the cytoplasmic region of MifM (Fig. 2f and Extended Data Fig. 9a). Taken together, these findings highlight the importance of the positive charge in the groove for the membrane insertion of MifM and Pf3 coat by YidC, while the conserved polar residues are probably important for creating the hydrophilic environment in the groove.

Several single-spanning membrane proteins, including MifM and Pf3 coat, harbor acidic residues on their N-terminal extracellular tails. Thus, the present results suggested that these acidic residues may interact with the Arg residue in the hydrophilic groove of YidC. To address this possibility, we examined the importance of these acidic

residues by an *in vivo* genetic analysis (Extended Data Fig. 9a). Although the effects of mutations of acidic residues in Pf3 coat were less pronounced than those in MifM, the results indicated that the mutations of the acidic residues in both MifM and Pf3 coat negatively affect their membrane insertion efficiencies, which supports our hypothesis (Extended Data Fig. 9b). To further confirm the direct interaction between the substrate and the hydrophilic groove, we performed an *in vivo* site-directed UV crosslinking analysis, using *p*-benzoyl-L-phenylalanine (pBpa)[22]. pBpa was introduced into the positions of either Gln187 or Trp244 in the groove, and those of Ala74 or Ile249 on the exterior surface of BhYidC (Fig. 2c and Extended Data Fig. 1). *E. coli* cells co-expressing MifM and the pBpa variant of BhYidC were irradiated by UV, and then the products cross-linked with MifM were analyzed by immunoblotting. We detected cross-linked products only for positions 187 and 244, suggesting that the groove can interact with MifM (Fig. 3). Altogether, these observations suggested that the site around Arg72 in the hydrophilic groove serves as the substrate-binding site, by recognizing the hydrophilic residues of the substrate, such as the acidic residues in the MifM and Pf3 coat proteins.

Based on the present structural and functional analyses, we propose a possible mechanism for the insertion of single-spanning membrane proteins with an acidic

N-terminal extracellular region, such as MifM and Pf3 coat, mediated by monomeric YidC (Fig. 4). In this mechanism, the substrate protein initially interacts with the C1 region (Fig. 4a), and then is transiently captured in the hydrophilic groove of YidC. This substrate binding may induce structural changes in the hydrophilic groove, to accommodate the various substrate proteins. In this context, the conserved Arg in the groove may participate in the substrate recognition (Fig. 4b). Subsequently, the TM region in the substrate protein is released into the membrane, with the hydrophilic residues translocated to the extracellular side. The substrate release may be facilitated by the hydrophobic interaction between the TM region and the lipid aliphatic chains. The membrane potential may also facilitate this process, by attracting the negative charge of the extracellular tail[23,24] (Fig. 4c).

Although the above mechanism clearly explains the insertion of a certain class of membrane proteins, i.e., single-spanning membrane proteins with an acidic N-terminal extracellular region, it cannot account for the insertion mechanism of other classes of membrane proteins with insertion mediated by YidC. For example, in *E. coli* YidC, the deletion of the C1 region or the simultaneous Ser-substitution of five amino acids, including the conserved Arg residue, reportedly did not impair the insertion activity of an M13 procoat derivative, a double-spanning membrane

protein[25]. Therefore, it is likely that these membrane proteins are inserted by a different mechanism, which may involve other sites in the hydrophilic groove than the Arg residue or transient oligomer formation by YidC. Further structural and biological studies are required to clarify the mechanism of the YidC-mediated insertion of these classes of membrane proteins.

Methods Summary

Histidine-tagged *Bacillus halodurans* YidC2 (BhYidC) was overproduced in *E. coli*, solubilized from the membrane with n-dodecyl-β-D-maltoside and cholesteryl hemisuccinate, and purified by successive Ni-NTA and gel filtration chromatography steps. The histidine tag was cleaved by TEV protease after Ni-NTA chromatography. Crystals were grown in a lipidic cubic phase, using monoolein. Diffraction data were collected on beamline BL32XU at SPring-8. The structure of YidC was determined by the multi-wavelength anomalous diffraction method, using the Hg-derivatized BhYidC (Y150C mutant) crystal, and was refined to R_{work}/R_{free} of 24.2%/25.9% at 2.4 Å resolution. The molecular dynamics simulation of YidC in the explicit POPE lipid bilayer was performed with the program NAMD 2.8 for 1,000 ns. The MifM insertion activity of YidC was analyzed by the MifM-based assay, in which the β-galactosidase (LacZ) activity of the *yidC2-lacZ* translational fusion increases in response to a defect in the SpoIIIJ-dependent insertion of MifM. The growth complementation assay was performed using *B. subtilis* mutant cells, in which the *yidC2* gene on the chromosome was disrupted and the *spoIIIJ* gene was mutated, with rescue by the plasmid harboring the wild-type IPTG-inducible *spoIIIJ* gene. *In vivo* photo-crosslinking was performed using *p*-benzoyl-L-phenylalanine (pBpa). *B. subtilis* MifM and pBpa variants of

BhYidC were overexpressed in *E. coli*, and the cells were irradiated by UV. BhYidC was then purified by Ni-NTA chromatography, and the products cross-linked with MifM were detected by immunoblotting.

References

1. Funes, S., Kauff, F., van der Sluis, E. O., Ott, M. & Herrmann, J. M. Evolution of YidC/Oxa1/Alb3 insertases: three independent gene duplications followed by functional specialization in bacteria, mitochondria and chloroplasts. *Biol. Chem.* **392,** 13–9 (2011).

2. Saller, M. J., Wu, Z. C., de Keyzer, J. & Driessen, A. J. M. The YidC/Oxa1/Alb3 protein family: common principles and distinct features. *Biol. Chem.* **393,** 1279–90 (2012).

3. Samuelson, J. C. *et al.* YidC mediates membrane protein insertion in bacteria. *Nature* **406,** 637–41 (2000).

4. Scotti, P. A *et al.* YidC, the Escherichia coli homologue of mitochondrial Oxa1p, is a component of the Sec translocase. *EMBO J.* **19,** 542–9 (2000).

5. Dalbey, R. E., Wang, P. & Kuhn, A. Assembly of bacterial inner membrane proteins. *Annu. Rev. Biochem.* **80,** 161–87 (2011).

6. Park, E. & Rapoport, T. A. Mechanisms of Sec61/SecY-mediated protein translocation across membranes. *Annu. Rev. Biophys.* **41,** 21–40 (2012).

7. Van den Berg, B *et al.* X-ray structure of a protein-conducting channel. *Nature* **427,** 36–44 (2004).

8. Tsukazaki, T. *et al.* Conformational transition of Sec machinery inferred from bacterial SecYE structures. *Nature* **455,** 4–6 (2008).

9. Nagamori, S., Smirnova, I. N. & Kaback, H. R. Role of YidC in folding of polytopic membrane proteins. *J. Cell Biol.* **165,** 53–62 (2004).

10. Wagner, S. *et al.* Biogenesis of MalF and the MalFGK(2) maltose transport complex in Escherichia coli requires YidC. *J. Biol. Chem.* **283,** 17881–90 (2008).

11. Yi, L. *et al.* YidC is strictly required for membrane insertion of subunits a and c of the F(1)F(0)ATP synthase and SecE of the SecYEG translocase. *Biochemistry* **42,** 10537–44 (2003).

12. Du Plessis, D. J. F., Nouwen, N. & Driessen, A. J. M. Subunit a of cytochrome o oxidase requires both YidC and SecYEG for membrane insertion. *J. Biol. Chem.* **281,** 12248–52 (2006).

13. Price, C. E. & Driessen, A. J. M. Conserved negative charges in the transmembrane segments of subunit K of the NADH:ubiquinone oxidoreductase determine its dependence on YidC for membrane insertion. *J. Biol. Chem.* **285,** 3575–81 (2010).

14. Serek, J. *et al.* Escherichia coli YidC is a membrane insertase for Sec-independent proteins. *EMBO J.* **23,** 294–301 (2004).

15. Facey, S. J., Neugebauer, S. A., Krauss, S. & Kuhn, A. The mechanosensitive channel protein MscL is targeted by the SRP to the novel YidC membrane insertion pathway of Escherichia coli. *J. Mol. Biol.* **365,** 995–1004 (2007).

16. Kohler, R. *et al.* YidC and Oxa1 form dimeric insertion pores on the translating ribosome. *Mol. Cell* **34,** 344–53 (2009).

17. Seitl, I., Wickles, S., Beckmann, R., Kuhn, A. & Kiefer, D. The C-terminal regions of YidC from Rhodopirellula baltica and Oceanicaulis alexandrii bind to ribosomes and partially substitute for SRP receptor function in Escherichia coli. *Mol. Microbiol.* **91,** 408–21 (2014).

18. Lotz, M., Haase, W., Kühlbrandt, W. & Collinson, I. Projection structure of yidC: a conserved mediator of membrane protein assembly. *J. Mol. Biol.* **375,** 901–7 (2008).

19. Kedrov, A. *et al.* Elucidating the native architecture of the YidC: Ribosome complex. *J. Mol. Biol.* **425,** 4112–24 (2013).

20. Krüger, V. *et al.* The mitochondrial oxidase assembly protein1 (Oxa1) insertase forms a membrane pore in lipid bilayers. *J. Biol. Chem.* **287,** 33314–26 (2012).

21. Chiba, S., Lamsa, A. & Pogliano, K. A ribosome-nascent chain sensor of membrane protein biogenesis in Bacillus subtilis. *EMBO J.* **28,** 3461–75 (2009).

22. Mori, H. & Ito, K. Different modes of SecY-SecA interactions revealed by site-directed in vivo photo-cross-linking. *Proc. Natl. Acad. Sci. U. S. A.* **103,** 16159–64 (2006).

23. Chen, M. *et al.* Direct interaction of YidC with the Sec-independent Pf3 coat protein during its membrane protein insertion. *J. Biol. Chem.* **277,** 7670–5 (2002).

24. Zhu, L. L., Wasey, A., White, S. H. & Dalbey, R. E. Charge-composition features of model single-span membrane proteins that determine selection of YidC and SecYEG translocase pathways in Escherichia coli. *J. Biol. Chem.* **288,** 7704–16 (2013).

25. Jiang, F. *et al.* Defining the regions of Escherichia coli YidC that contribute to activity. *J. Biol. Chem.* **278,** 48965–72 (2003).

Supplementary Information is linked to the online version of the paper at www.nature.com/nature.

Acknowledgements

We thank K. Watanabe from Shoko Scientific Inc. for assistance with the SEC-MALLS experiments; T. Nishizawa, T. Higuchi, H.E. Kato, M. Hattori, R. Ishii

and H. Nishimasu for useful discussions; A. Kurabayashi, H. Nakamura, S. Hibino, T. Takino and C. Tsutsumi for technical support; A. Nakashima and R. Yamazaki for secretarial assistance; the RIKEN BioResource Center (Ibaraki, Japan) for providing *Bacillus halodurans* genomic DNA; the RIKEN Integrated Cluster of Clusters (RICC) for providing computational resources; and the beamline staff members at BL32XU of SPring-8 (Hyogo, Japan) for technical assistance during data collection. The synchrotron radiation experiments were performed at BL32XU of SPring-8 (proposal Nos. 2011A1125, 2011A1139, 2011B1062, 2011B1280, 2012A1093, 2012A1201, 2012B1146, 2012B1162, 2013A1128), with approval from RIKEN. This work was supported by Platform for Drug Discovery, Informatics, and Structural Life Science from the Ministry of Education, Culture, Sports, Science and Technology (MEXT), by JSPS KAKENHI (Grant Nos. 20247020, 20523517, 24687016, 24102503, 24121704, 24227004, 24657095, 25291006, 25291009, 25660073), by FIRST program, by PRESTO, JST, by a Grant-in-Aid for JSPS Fellows, by a grant for HPCI STRATEGIC PROGRAM Computational Life Science and Application in Drug Discovery and Medical Development from MEXT, and by grants from Private University Strategic Research Foundation Support Program (MEXT), Nagase Science and Technology Foundation, and Astellas Foundation for Research on Metabolic Disorders.

Author Contributions

K.K. performed the crystallization and structure determination. S.C. performed the genetic analyses. K.K., A.F., K.N., Y. Sugano, A.D.M., Y.T., H.M. and T.T. performed the functional analysis. M.T., T.M., Y. Sugita and R.I. performed the MD simulation. K.K., N.D. and F.A. identified the molecular mass. K.H., Y.N., R.I., T.T. and O.N. assisted with the structure determination. K.K., S.C., K.I., R.I., T.T. and O.N. wrote the manuscript. T.T. and O.N. directed and supervised all of the research.

Author Information

The atomic coordinates and structure factors for BhYidC$_{27–266}$ and BhYidC$_{27–267}$ have been deposited in the Protein Data Bank, under the accession codes 3WO6 and 3WO7, respectively. The authors declare no competing financial interests. Reprints and permissions information is available at www.nature.com/reprints. Correspondence and requests for materials should be addressed to O.N. (nureki@biochem.s.u-tokyo.ac.jp) or T.T. (ttsukaza@bs.naist.jp).

Figure Legends

Figure 1| Overall structure.

a, Cartoon representations of BhYidC, viewed from the membrane and extracellular sides. The structure is colored blue to red from the N to C terminus. **b**, Surface model representations of BhYidC colored by the electrostatic potential, ranging from blue (+20 kT/e) to red (−20 kT/e). **c**, Topology diagram of BhYidC, colored as in (**a**). **d**, Cut-away molecular surface representations, viewed from the membrane side.

Figure 2| *In vivo* functional analyses of YidC.

a, **d-f**, Efficiencies of MifM and Pf3-MifM membrane insertion determined by LacZ activities (Miller units; mean ± SD, n = 3) in the *spoIIIJ* mutants. K248stop represents a *spoIIIJ* derivative, which has a stop codon introduced at the 248th position. Their accumulation in the cell is shown (lower panel). **b**, Growth complementation of *B. subtilis* cells reliant on chromosomal SpoIIIJ mutant in the absence of isopropyl β-D-thiogalactopyranoside (IPTG). **c**, Close-up view of the hydrophilic groove, showing the side chains of the highlighted residues. The corresponding residues in SpoIIIJ are indicated in parentheses.

Figure 3| Substrate binding to the hydrophilic groove.

In vivo photo-crosslinking between the hydrophilic groove of BhYidC and MifM. The pBpa positions introduced into BhYidC are indicated. Ni-NTA purified membrane proteins were analyzed by SDS-PAGE, and BhYidC-FLAG-His_8 and MifM were detected by immunoblotting. The ~40 kDa-bands are attributed to cross-linked products of BhYidC with MifM and unidentified endogenous proteins, as indicated by YidC-X. The accumulation of MifM in the membrane is shown (lower panel).

Figure 4| Proposed model for membrane insertion of a single spanning protein.

a–d, The present crystal structure probably represents the resting state before substrate binding. The hydrophilic region of the substrate may be transiently captured in the hydrophilic groove of YidC, resulting in the substrate-bound state (**a**, **b**). Substrate release into the membrane may be facilitated by the hydrophobic interaction between the TM region and the lipid aliphatic chains, as well as the membrane potential ($\Delta\psi$), attracting the negatively charged residue of the extracellular region by electrophoretic force (**c**, **d**).

Methods

Cloning, expression and purification for structure determination

Bacillus halodurans YidC2 (BhYidC) was cloned into a pET-modified vector[26]. The resulting two plasmids, encoding BhYidC(1–26)-H_8-ENLYFQGQ-BhYidC(27–266) ($BhYidC_{27–266}$) and BhYidC(1–26)-ENLYFQGQ-BhYidC(27–267)-LESSV-ENLYFQGQ-GFP-H_8 ($BhYidC_{27–267}$), were expressed in *E. coli* C41 (DE3) cells harboring pRARE (Novagen), and the proteins were purified by the following protocol. The cells were grown in a 5 L culture at 37 °C to an A_{600} of 0.7, induced with 1 mM isopropyl β-D-thiogalactopyranoside (IPTG) at 15 °C for 16 h, harvested by centrifugation, resuspended in buffer containing 20 mM Tris-HCl, pH 8.0, and 0.1 mM phenylmethylsulfonyl fluoride, and disrupted by two passages through a Microfluidizer (Microfluidics) at 15,000 p.s.i. After removal of the debris by low speed centrifugation, the supernatant was ultra-centrifuged (138,000 g, 1 h) to pellet the membranes, which were then solubilized in a buffer containing 300 mM NaCl, 20 mM Tris-HCl, pH 8.0, 20 mM imidazole, 1% *n*-dodecyl-β-D-maltoside (DDM), and 0.1% cholesteryl hemisuccinate (CHS). Insoluble materials were removed by ultra-centrifugation

(138,000 g, 30 min), and the supernatant was mixed with Ni-NTA Superflow (QIAGEN). After binding for 1 h, the resin was washed with 300 mM NaCl, 20 mM Tris-HCl, pH 8.0, 20 mM imidazole, 0.1% DDM, and 0.01% CHS, and BhYidC was eluted with the same buffer supplemented with 300 mM imidazole. The N-terminal residues and the His_8-tag or GFP-His_8-tag were cleaved by His-tagged TEV protease (laboratory stock), and the sample was reloaded onto the Ni-NTA column to remove the protease. The flow-through fraction containing BhYidC was collected, concentrated, and further purified by size-exclusion chromatography in 300 mM NaCl, 20 mM Tris-HCl, pH 8.0, 0.1% DDM, and 0.01% CHS. For crystallization, the purified protein was concentrated to 6 mg ml^{-1} with a centrifugal filter device (Millipore, 50kDa MW cutoff), and dialyzed against a solution containing 1 mM Tris-HCl, pH 8.0, 0.05% DDM, and 0.005% CHS. For mercury derivatization, the Y150C $BhYidC_{27–266}$ mutant was purified and incubated with 2 mM methyl mercury chloride for 1 h before crystallization.

Crystallization and heavy-atom derivatization

The protein was mixed with monoolein in a 2:3 protein to lipid ratio (w/w), using the twin-syringe mixing method[27]. Aliquots (50 nl) of the protein-LCP mixture were

spotted on a 96-well sandwich plate and overlaid with 800 nl of precipitant solution using a crystallization robot, mosquito LCP (TTP LabTech). The crystals of BhYidC$_{27–266}$ and BhYidC$_{27–267}$ were grown at 20 °C in reservoir solutions containing 28–32% PEG500DME, 2.5 mM $CdCl_2$, and 100 mM Na-$(CH_3)_2AsO_2$, pH 6.0; and 24–26% PEG500DME, 10 mM $CuCl_2$, 200 mM NH_4COOH, and 100 mM MES-NaOH, pH 6.0, respectively. The heavy atom derivative crystals were obtained by co-crystallization of the Y150C mutant and methyl mercury chloride in the same reservoir solution used for the BhYidC$_{27–266}$ crystals. The crystals grew to full size in 2-3 weeks. The crystals were flash-cooled, using reservoir solution supplemented with 20% PEG500DME and 20% glycerol as a cryoprotectant, and stored in liquid nitrogen.

Data collection and structure determination

X-ray diffraction data sets were collected by the helical data collection method on beamline BL32XU at SPring-8, using a micro beam with a 1 μm width and a 10 μm height[28]. Diffraction data were processed using HKL2000 (HKL Research Inc.) or XDS[29]. One Hg site was identified with the program SHELXD[30]. The initial phases were calculated using SHARP[31], followed by solvent flattening with SOLOMON[32]. The main chain was traced by automated model building using RESOLVE[33]. The model was

further built manually using COOT[34] and refined using PHENIX[35]. The structures of $BhYidC_{27–266}$ and $BhYidC_{27–267}$ were determined by molecular replacement, using the program PHASER[36]. The Ramachandran plots were calculated with RAMPAGE[37]. Data collection and refinement statistics are provided in Extended Data Table 1. The $BhYidC_{27–266}$ crystal contains one molecule in the asymmetric unit. The $BhYidC_{27–267}$ crystal contains two molecules in the asymmetric unit (Mol A and Mol B), but they do not form a face-to-face dimer. The figures of the molecular structures were prepared using CueMol (http://www.cuemol.org/).

Bacterial strains and plasmids for *in vivo* functional analysis

B. subtilis strains, plasmids, and DNA oligonucleotides are listed in Supplementary Tables 1–3, and were constructed as described in the Supplementary Information.

β-galactosidase activity assay and immunoblotting

B. subtilis cells were cultured at 37 °C in LB or CH medium. Aliquots (500 μl) of cultures at OD_{600} = ~0.5 were harvested and used for β-galactosidase activity assays and immunoblotting. The β-galactosidase activities were measured as described

previously[38,39]. For immunoblotting, a 500 µl aliquot of the culture was mixed with 56 µl of 50% trichloroacetic acid and incubated on ice for at least 5 min. The cells were precipitated by centrifugation (4 °C, 15,000 rpm, 5 min), washed with 1 ml of 1 M Tris-HCl, pH 8.0, resuspended in SB buffer (33 mM Tris-HCl, pH 8.0, 40% sucrose, 1 mM EDTA) containing 1 mg/ml lysozyme (Sigma), and incubated at 37 °C for 10 min. The cells were then solubilized by adding an equal volume of 2xSDS-loading buffer and subjected to immunoblotting, using either anti-FLAG (Sigma) or anti-BsSpoIIIJ, as described previously[40]. Antiserum production is described in the Supplementary Information.

Growth complementation assay

B. subtilis cells were cultured at 37 °C in LB medium, containing 100 µg/ml spectinomycin and 1 mM IPTG. Aliquots (3.5 µl) of serially diluted (10^{-1}–10^{-5}), fully grown cultures were spotted on LB-spectinomycin agar plates with or without 1 mM IPTG, and incubated at 37 °C for 15 h.

***In vivo* photo-crosslinking assay**

BhyidC-FLAG®(SIGMA-ALDRICH)-*His*$_8$ and *BsmifM* were cloned into the *Nco*I and *Bam*HI sites of MCS1 and the *Nde*I and *Xho*I sites of MCS2 in pETDuet (Novagen), respectively. An amber mutation, TAG, in *BhyidC* was introduced by site-directed

mutagenesis. *BsmifM*-deletion plasmids were generated by restriction digestion of the plasmids with *Sal*I and *Xho*I and ligation. *E. coli* BL21 (DE3) cells harboring two plasmids, pEVOL-pBpF (addgene) and a pETDuet-based plasmid expressing BhYidC and BhMifM, were grown at 37˚C in M9-glucose medium supplemented with pBpa (1 mM)[22] and appropriate antibiotics until mid-log phase, and then induced with 1 mM IPTG for 30 min. Portions (1 ml for isolation of total membranes and 2 ml for purification of YidC by Ni-NTA chromatography) of the culture were transferred to a dish and irradiated with UV (365 nm) for 5 min, by using a B-100AP (UVP) UV lamp at a distance of 5 cm. The irradiated cells were collected by centrifugation, suspended in 300 μL of 10 mM Tris-HCl buffer, pH 8.0, containing 1 mM EDTA-Na and 0.1 mM 4-(2-aminoethyl)benzenesulfonyl fluoride hydrochloride, and disrupted by freeze-thawing and sonication (Qsonica) with cooling on ice. The cellular debris was separated by centrifugation at 9,000 g for 1 min and used for the isolation of total membranes or the purification of YidC. Total membranes were isolated by ultracentrifugation at 100,000 g for 20 min. For the purification of YidC, the membrane proteins were solubilized in SC buffer, containing 20 mM Tris-HCl, pH 8.0, 300 mM NaCl, 20 mM imidazole-HCl (pH 8.0), 1% DDM, 0.1% CHS and 0.1 mM 4-(2-aminoethyl)benzenesulfonyl fluoride hydrochloride, for 30 min at 4˚C. Insoluble

materials were removed by ultracentrifugation at 100,000 g for 20 min. The supernatant was mixed with Ni-NTA Agarose (Qiagen) pre-equilibrated with SC buffer. After binding for 30 min, the resin was washed with SC buffer containing 0.1% DDM, and then YidC was eluted with SC buffer supplemented with 300 mM imidazole-HCl (pH 8.0). Proteins were separated by SDS-PAGE and detected by immunoblotting, using anti-FLAG (Sigma) or anti-BsMifM[40] antibodies.

Molecular dynamics simulation

The simulation system included BhYidC, phosphoryloleoyl phosphatidylethanolamine (POPE), water molecules, and 150 mM sodium chloride. At first, the position and orientation of BhYidC in the POPE lipid bilayer were optimized using the implicit solvent and membrane models (T.M. and Y. Sugita, manuscript in preparation). Next, the disordered region in the C2 loop (residues 200–213) was modeled, using the program Modeller[41]. The missing atoms, including hydrogens in the protein, were built with the program VMD[42]. Finally, the periodic boundary system, including the explicit solvent and the POPE lipid bilayer[43], was prepared. The resulting size of the simulation box was 96 (Å) × 96 (Å) × 96 (Å). The

net charge of the solute was neutralized through the addition of chloride and sodium ions. The molecular topologies and parameters from Charmm36 were used[43].

Molecular dynamics simulations were performed with the program NAMD 2.8[44]. The system was first energy minimized for 1,000 steps with fixed positions of the non-hydrogen atoms, and then for another 1,000 steps with 10 kcal/mol restraints for the non-hydrogen atoms. Next, we performed the long equilibration run of 50 ns under NVT conditions, with 10 kcal/mol restraints for protein non-hydrogen atoms and 0.1 kcal/mol restraints for water molecules, to optimize the locations of the lipid molecules around the protein, especially the hydrophilic groove. Finally, equilibration was performed for 5 ns under NPT conditions, with 10 and 0.1 kcal/mol restraints for the protein main chain and side chain atoms, respectively. The production process was performed for 1,000 ns. During the equilibration and production processes, the pressure and temperature were set to 1.0 atm and 300 K, respectively. Constant temperature was maintained by using Langevin dynamics. Constant pressure was maintained by using the Langevin piston Nose-Hoover method[45]. Long-range electrostatic interactions were calculated using the particle mesh Ewald method[46].

Determination of the molecular mass of YidC in detergent solution by

SEC-MALLS

The instrument setup used for the SEC-MALLS experiment consisted of a Prominence HPLC system (Shimadzu) with an SPD-20A ultraviolet absorbance detector connected in series with a DAWN HELEOS II light-scattering detector (Wyatt Technology) and an OPTILAB T-rEX differential refractive index detector (Wyatt Technology). Analytical size-exclusion chromatography was performed using a Superdex 200 10/300 column (GE Healthcare) equilibrated with buffer containing 300 mM NaCl, 20 mM Tris-HCl, pH 8.0, 0.1% DDM, and 0.01% CHS. The purified $BhYidC_{27–266}$ (60 µg) was injected into the column, and the elution was monitored in-line with the three detectors. A 658.0-nm wavelength laser was used in the light scattering experiment. The data were corrected for the volume delay of UV between the other detectors and were analyzed using the ASTRA software (Wyatt Technology). The molecular masses of the protein–micelle complex, the micelle and the protein were determined as described[47,48]. The dn/dc value of the mixture of DDM and CHS in buffer, containing 300 mM NaCl and 20 mM Tris-HCl, pH 8.0, was determined off-line using an OPTILAB T-rEX refractometer with a 658.0-nm wavelength laser, as described[49].

Extended Data Figure Legends

Extended Data Table 1| Data collection and refinement statistics

Extended Data Figure 1| Multiple amino acid sequence alignment of YidCs.

Sequence alignment of *Bacillus halodurans* YidC2 (BhYidC2), *B. halodurans* YidC1 (BhYidC1), *Bacillus subtilis* SpoIIIJ (BsSpoIIIJ), *B. subtilis* YidC2 (BsYidC2) and *Escherichia coli* YidC (EcYidC). The secondary structure of $BhYidC_{27–266}$ is indicated above the sequences. Alpha-helices (described in the main text) and beta-strands (ES1 and ES2 in the E2 region) are indicated by cylinders and arrows, respectively. Strictly conserved residues among the five species are highlighted in red boxes, and highly conserved residues are indicated by red letters. The hydrophilic and bulky residues that were mutated, and the pBpa positions introduced into BhYidC are indicated by grey, green, and blue triangles, respectively. The *spoIIIJ-K248stop* derivative has a stop codon introduced at the 248th position, as indicated, and thereby expresses a SpoIIIJ mutant that lacks the C-terminal 14 residues.

Extended Data Figure 2| Electron density map of BhYidC.

Stereo view of the $2m|\mathbf{F}|_o - D|\mathbf{F}|_c$ electron density map of the TM2 helix, contoured at 1.1 σ.

Extended Data Figure 3| Monomeric YidC.

a, The crystal packing of $BhYidC_{27–266}$, viewed from the plane of the membrane. The molecule in the asymmetric unit is colored red. **b**, The crystal packing of $BhYidC_{27–267}$, viewed from the plane of the membrane. There are two molecules (Mol A in light pink and Mol B in light blue) in the asymmetric unit. **c,** The chromatograms show the ultraviolet (UV), refractive index (RI) and light scattering (LS) detector readings. The volume delays of UV between the other detectors were corrected. The traces were normalized to the peak maxima. The green and blue lines in the LS chromatogram indicate the calculated molecular masses of the protein-detergent complex and the protein, respectively. **d**, The RI of the mixture was measured in response to 5 concentration steps. The dn/dc value of the mixture of DDM and CHS was determined using linear regression of the RI versus the concentration. **e**, The molecular mass values determined by SEC-MALLS and calculated from the amino acid sequence.

Extended Data Figure 4| Structural flexibility of the hydrophilic groove and C1 region.

a, **b**, Superimposition of the crystal structures of $BhYidC_{27–266}$ (colored) and Mol B of

BhYidC$_{27–267}$ (gray), viewed from the membrane (**a**) and extracellular (**b**) sides. The conformational changes observed in CH1 and CH2 are indicated by black arrows. **c**, Close-up view of the C1 region. The side chains of Pro111 are shown by stick models. In the BhYidC$_{27–267}$ structure, the arrangement of the C1 region with respect to the core region is rotated by ~35˚, as compared with that in the BhYidC$_{27–266}$ structure. As a result, the tip of the C1 region is displaced by ~10 Å in the BhYidC$_{27–267}$ structure. **d**, Close-up views of the hydrophilic groove (left panel: BhYidC$_{27–266}$, right panel: Mol B of BhYidC$_{27–267}$). The distances between the Cα atoms of Cys136 and Met221 are indicated by dashed lines.

Extended Data Figure 5| The hydrophobic core of BhYidC.

a, The crystallographic B-factors are colored in a gradient varying from blue to red, representing 30 to 140 Å^2. **b**, **c**, Stereo views of the hydrophobic core, showing the side chains of the hydrophobic residues.

Extended Data Figure 6| MD simulation of BhYidC for 1 μs in a lipid bilayer.

a, Snapshots of the structure over the time course of the simulation at 400 ns intervals: 0

ns (blue), 400 ns (magenta) and 800 ns (light green). **b**, Root mean square fluctuation (RMSF) of BhYidC during the simulation. The secondary structure of BhYidC is indicated below the line. **c**, The water probability density map in the simulation, contoured at 0.001 molecules/$Å^3$·ns.

Extended Data Figure 7| Gene structures of strains and YidC mutants used for *in vivo* genetic analyses.

a, Schematic representations of the gene structures of the *yidC2-lacZ* reporter strains used for the MifM-based assay. "*spoIIIJ*-(flag)*" indicates either wild type or mutant *spoIIIJ*. "*yidC2-lacZ*" represents a translational gene fusion with the *lacZ* sequence in frame after the 6th codon of *yidC2*. The native *mifM-yidC2* on the chromosome remained intact. **b**, Deleted regions of SpoIIIJ, viewed from the extracellular side. Residue numbers in SpoIIIJ are indicated. Δ92–126-GG represents the mutant in which the entire C1 region is replaced by a Gly-Gly linker. Δ97–103/114–120 represents the mutant in which both the CH1 and CH2 helices are shortened by 7 residues. **c**, Schematic representations of the gene structures used for growth complementation assays. SpoIIIJ becomes growth-essential for *B. subtilis* when *yidC2* is disrupted. Cells with a disruption of the chromosomal *yidC2* were transformed with the rescue plasmid

pCH1805, which expresses wild type *spoIIIJ-flag* under the control of the IPTG-inducible Pspac promoter. The native *spoIIIJ* on the chromosome was replaced by either wild type or mutant *spoIIIJ* (*spoIIIJ***-(flag)*). In the absence of IPTG, *spoIIIJ-flag* is not expressed from the plasmid, making the chromosomal *spoIIIJ***-(flag)* the only source of cellular YidC. The complementation test measures the global role of SpoIIIJ to insert a wide range of membrane proteins, including single- and multi-spanning membrane proteins.

Extended Data Figure 8| Schematic explanation of the β-galactosidase activity assay for MifM insertion activity.

a, **b**, MifM is a single-spanning membrane protein, and its membrane insertion is considered to be mediated by YidC/SpoIIIJ[21]. To evaluate the MifM insertion activity of SpoIIIJ, we performed a genetic analysis using *B. subtilis.* In *B. subtilis,* SpoIIIJ is constitutively expressed, while YidC2 is expressed only when the SpoIIIJ activity is compromised, by the following mechanism. The expression of *yidC2* is regulated by its upstream cis-regulator ORF of *mifM,* which is cotranscribed with *yidC2.* During the synthesis of MifM, the C-terminal region of nascent MifM interacts with the peptide

exit tunnel of ribosome and causes translational arrest[40,50]. When the SpoIIIJ activity is normal, the translational arrest is released by the SpoIIIJ-dependent membrane insertion of MifM. Therefore, the translational arrest is transient or does not occur (**a**). In contrast, when SpoIIIJ activity is compromised, MifM is not inserted into the membrane and its translation is arrested, which causes ribosome stalling. The stalled ribosome disrupts the downstream stem-loop structure and exposes the Shine-Dalgarno (SD) translation initiation signal sequence of the *yidC2* mRNA (**b**). Thus, we can estimate the *in vivo* SpoIIIJ activity by measuring the expression of the introduced *yidC2-lacZ* fusion (Extended Data Fig. 7a): the reduction of MifM insertion efficiency by SpoIIIJ elevates the LacZ activity[21,50].

Extended Data Figure 9| Effects of N-terminal negatively charged residues of substrates for insertion.

a, Schematic representations of the N-terminal negatively charged residues of the MifM and Pf3-MifM chimeric proteins. **b**, Membrane insertion efficiencies of MifM mutants and Pf3-MifM mutants. The efficiencies were determined by the LacZ activities (Miller units; mean ± SD, n = 3). The N-terminal negatively charged residues of MifM and Pf3-MifM and the numbers of the charged residues are shown at the bottom (EDD: wild

type MifM; DD: wild type Pf3-MifM). Mutations of the acidic residues in Pf3 coat had less pronounced effects than those in MifM, probably because the membrane insertion is facilitated by multiple interacting factors depending on the amino acid sequence.

Additional References

26. Nishizawa, T. *et al.* Structural Basis for the Counter-Transport Mechanism of a H^+/Ca^{2+} Exchanger. *Science* **341,** 168–72 (2013).

27. Caffrey, M. Crystallizing membrane proteins for structure determination: use of lipidic mesophases. *Annu. Rev. Biophys.* **38,** 29–51 (2009).

28. Hirata, K. *et al.* Achievement of protein micro-crystallography at SPring-8 beamline BL32XU. *J. Phys. Conf. Ser.* **425,** 012002 (2013).

29. Kabsch, W. XDS. *Acta Crystallogr. D. Biol. Crystallogr.* **66,** 125–32 (2010).

30. Schneider, T. R. & Sheldrick, G. M. Substructure solution with SHELXD. *Acta Crystallogr. D. Biol. Crystallogr.* **58,** 1772–9 (2002).

31. De la Fortelle, E., Irwin, J. J. & Bricogne, G. SHARP□: A Maximum-Likelihood Heavy-Atom Parameter Refinement Program for the MIR and MAD Methods. *Methods Enzym.* **276,** 472–94 (1997).

32. Abrahams, J. P. & Leslie, A. G. Methods used in the structure determination of bovine mitochondrial F1 ATPase. *Acta Crystallogr. D. Biol. Crystallogr.* **52,** 30–42 (1996).

33. Terwilliger, T. C. & Berendzen, J. Automated MAD and MIR structure solution. *Acta Crystallogr. D. Biol. Crystallogr.* **55,** 849–61 (1999).

34. Emsley, P., Lohkamp, B., Scott, W. G. & Cowtan, K. Features and development of Coot. *Acta Crystallogr. D. Biol. Crystallogr.* **66,** 486–501 (2010).

35. Adams, P. D. *et al.* PHENIX: a comprehensive Python-based system for macromolecular structure solution. *Acta Crystallogr. D. Biol. Crystallogr.* **66,** 213–21 (2010).

36. Adams, P. D. *et al.* PHENIX: building new software for automated crystallographic structure determination. *Acta Crystallogr. D. Biol. Crystallogr.* **58,** 1948–54 (2002).

37. Lovell, S. C. *et al.* Structure validation by Calpha geometry: phi,psi and Cbeta deviation. *Proteins* **50,** 437–50 (2003).

38. Miller, J. H. *Experiments in Molecular Genetics*. (Cold Spring Harbor Laboratory Press, 1972).

39. Rubio, A., Jiang, X. & Pogliano, K. Localization of translocation complex components in Bacillus subtilis: enrichment of the signal recognition particle receptor at early sporulation septa. *J. Bacteriol.* **187,** 5000–2 (2005).

40. Chiba, S. *et al.* Recruitment of a species-specific translational arrest module to monitor different cellular processes. *Proc. Natl. Acad. Sci. U. S. A.* **108,** 6073–8 (2011).

41. Sali, A. *et al.* Evaluation of comparative protein modeling by MODELLER. *Proteins* **23,** 318–26 (1995).

42. Humphrey, W., Dalke, A. & Schulten, K. VMD: visual molecular dynamics. *J. Mol. Graph.* **14,** 33–8, 27–8 (1996).

43. Klauda, J. B. *et al.* Update of the CHARMM all-atom additive force field for lipids: validation on six lipid types. *J. Phys. Chem. B* **114,** 7830–43 (2010).

44. Phillips, J. C. *et al.* Scalable molecular dynamics with NAMD. *J. Comput. Chem.* **26,** 1781–802 (2005).

45. Feller, S. E., Zhang, Y., Pastor, R. W. & Brooks, B. R. Constant pressure molecular dynamics simulation: The Langevin piston method. *J. Chem. Phys.* **103,** 4613 (1995).

46. Darden, T., York, D. & Pedersen, L. Particle mesh Ewald: An N·log(N) method for Ewald sums in large systems. *J. Chem. Phys.* **98,** 10089 (1993).

47. Hayashi, Y., Matsui, H. & Takagi, T. Membrane protein molecular weight determined by low-angle laser light-scattering photometry coupled with high-performance gel chromatography. *Methods Enzymol.* **172,** 514–28 (1989).

48. Slotboom, D. J., Duurkens, R. H., Olieman, K. & Erkens, G. B. Static light scattering to characterize membrane proteins in detergent solution. *Methods* **46,** 73–82 (2008).

49. Strop, P. & Brunger, A. T. Refractive index-based determination of detergent concentration and its application to the study of membrane proteins. *Protein Sci.* **14,** 2207–2211 (2005).

50. Chiba, S. & Ito, K. Multisite ribosomal stalling: a unique mode of regulatory nascent chain action revealed for MifM. *Mol. Cell* **47,** 863–72 (2012).

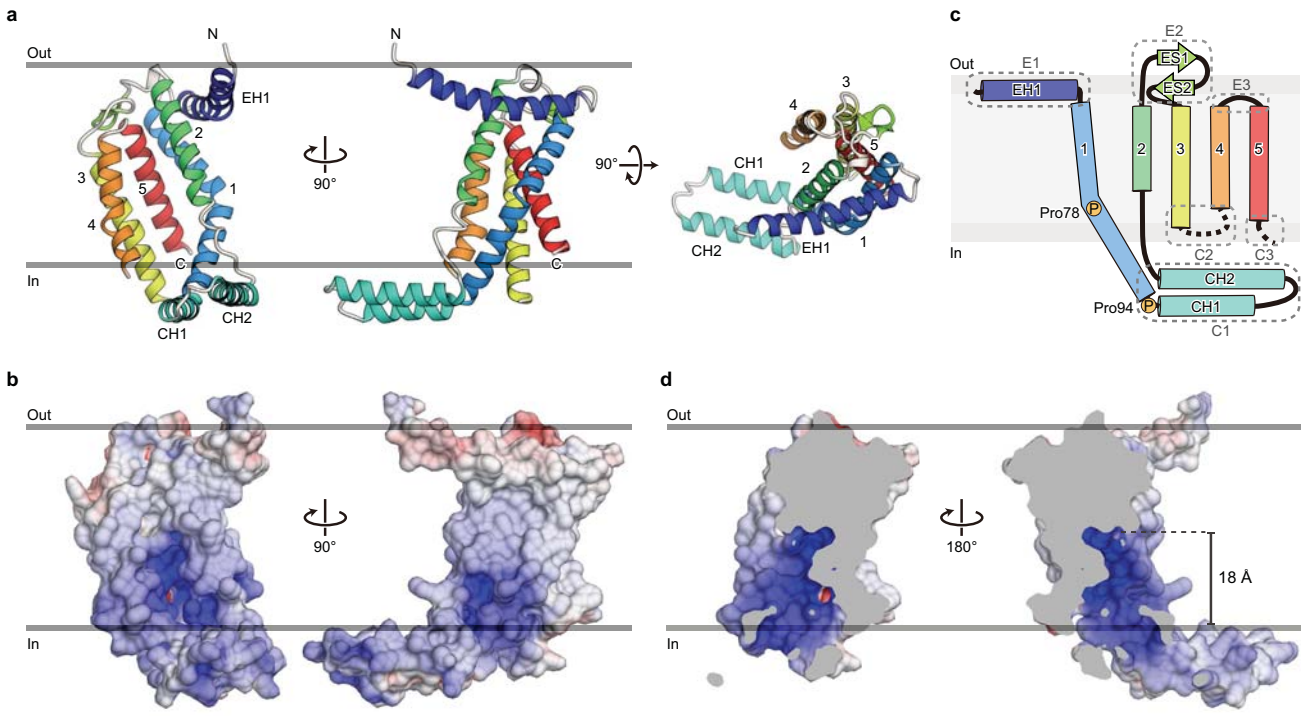

Kumazaki et al. Fig.1

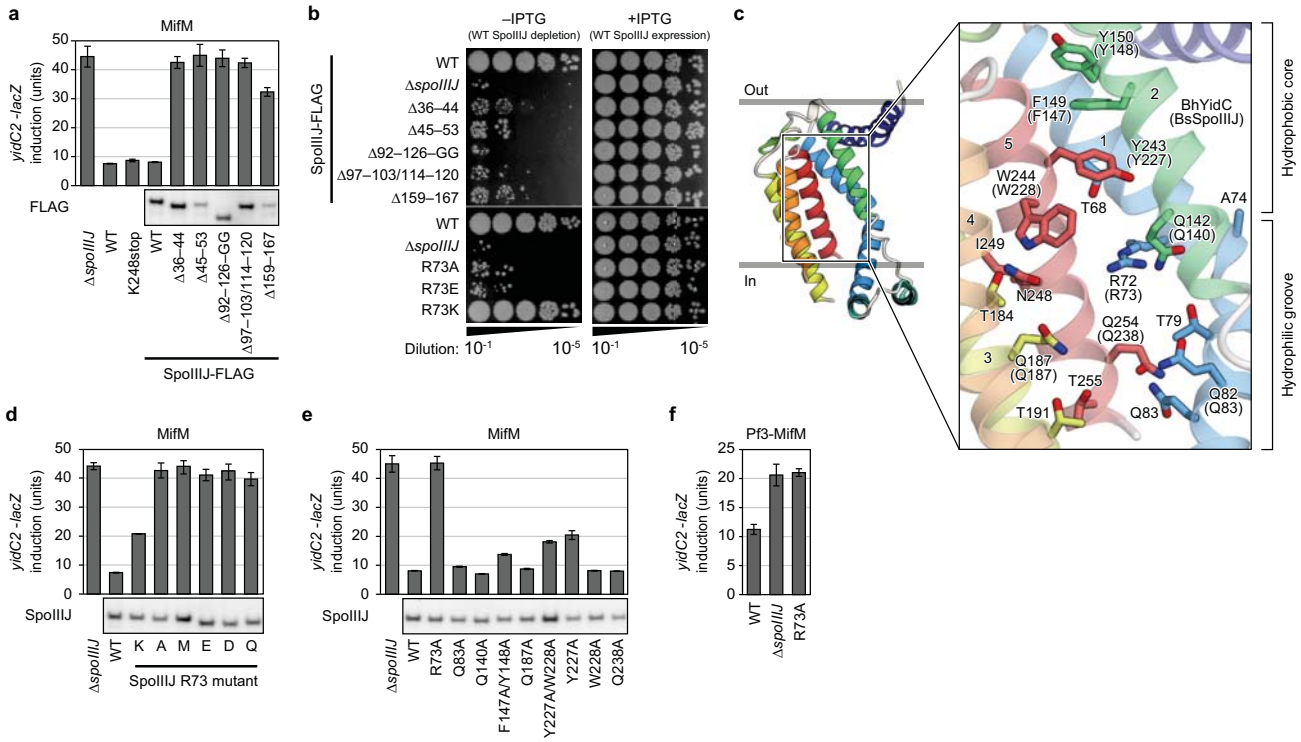

Kumazaki et al. Fig.2

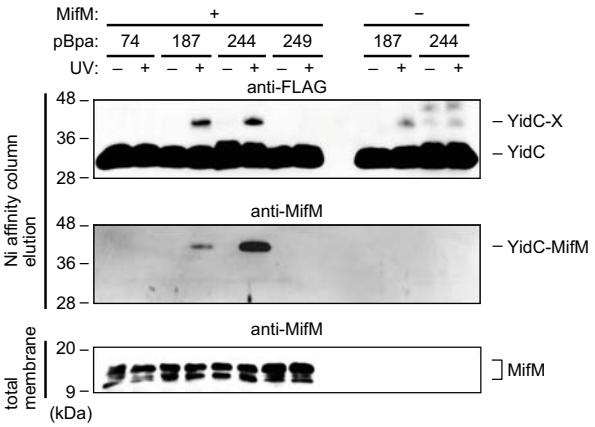

Kumazaki et al. Fig.3

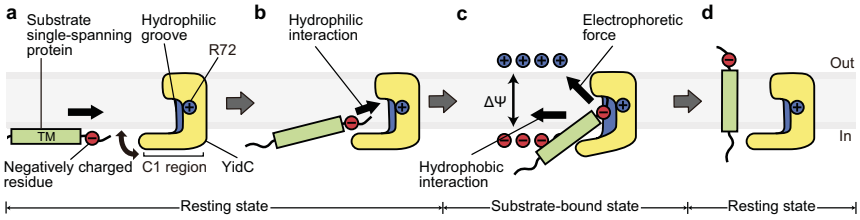

Kumazaki et al. Fig.4